Non-equilibrium phase field model using thermodynamics data estimated by machine learning for additive manufacturing solidification

Sukeharu Nomoto*, Masahito Segawa* and Hiroshi Wakameda*

*ITOCHU Techno-Solutions Corporation, 3-2-5, Kasumigaseki, Chiyoda-ku, Tokyo 100-6080 Japan

*Corresponding author
Email: sukeharu.nomoto@ctc-g.co.jp

Abstract

A multi-phase field method using finite interface dissipation model proposed by Steinbach et al. is applied to simulate solidification microstructure evolution of stainless steel composition in the non-equilibrium condition of high cooling rate and temperature gradient of additive manufacturing. The calculation is performed for quinary system in order to simulate solidification of engineering composition. Thermodynamic calculation using CALPHAD database in this multi-phase field method calculation is replaced by machine learning prediction procedure to reduce calculation time. The microstructure evaluated by using machine learning parameter is good agreement with one directly coupled with CALPHAD database. This calculation is approximately five times faster than the direct CALPHAD calculation method. Finally, it is confirmed that this multi-phase field method can be applicable to simulate non-equilibrium phase transformation of additive manufacturing condition with high numerical stabilization.

Introduction

Many authors apply Cellular Automata method or Monte Carlo model to simulate rapid solidification texture and grain evolution of additive manufacturing (AM) [1, 2]. However, it seems that these methodologies could not provide proper dendrite morphology according to the constitutional undercooling because of lack of interface driving force estimation derived from chemical potential. S. Ghosh et al. discussed microstructure evolution of solidification of Ni alloy in the condition of AM, high cooling rate and temperature gradient, on the basis of the classical solidification theory using three-dimensional finite element thermal analysis and phase-field method [3, 4]. It was confirmed that the relation between the primary dendrite arm spacing and cooling rate and temperature gradient follow the solidification theory equation. Furthermore, they discussed segregation behavior by comparing with the theoretical solute petitioning equation for rapid solidification interface. However, these studies were performed for binary, Ni-Nb, system. It is considered that development of multi-phase field method (MPFM) for multi-element, that is free of quasi-equilibrium in the interface for adapting rapid solidification, should be developed for applying these discussion to engineering alloy.

Multi-phase field method that proposed by Steinbach about twenty years ago has been applied to many numerical simulation fields [5]. MPFM coupled with CALPHAD database using TQ-Interface of Thermo-Calc [6] provides us to simulate microstructure evolution for many engineering metal alloy processes [7]. MPFM coupling with solving solute diffusion is based on the diffuse-interface model, in which equal diffusion potential or quasi-equilibrium is assumed in the interface region. It is also generally called as KKS model [8]. However, in practical calculation using CALPHAD database coupling, it consumes long time to obtain quasi-equilibrium concentration at all grid points in the interface region. Steinbach and Zhang proposed finite interface dissipation model, which was based on non-equal diffusion potential after that [9, 10]. It is called non-equilibrium multi-phase field model (NEMPFM) in this study. This method has another advantage to avoid iterating calculation obtaining quasi-equilibrium composition in the interface region. It leads to decreasing calculation time by comparing with that of MPFM. We developed CALPHAD database coupled NEMPFM program for practical engineering steel system [11].

However, NEMPFM using TQ-Interface spends huge time for the thermodynamics calculation for NEMPFM yet. Furthermore, it can perform only on Thermo-Calc usage permitted platform. In this study, we attempt to accelerate NEMPFM thermodynamics calculation by replacing CALPHAD database coupling method by linear prediction procedure of neural network as a machine-learning. The thermodynamics calculation consists of obtaining Gibbs free energy and chemical potential that are varied as functions of temperature and composition in the interface region. The mini-batch gradient descent method [12] is employed for neural network training, of which data, these values, are obtained from CALPHAD database coupled NEMPFM calculation result. The identified neural network parameters, bias and weight, are adapted to the linear prediction procedure in NEMPFM program. This method is applied to solidification simulation for quinary, Fe-Cr-Ni-Mo-C, stainless steel in conditions of high cooling rate and thermal gradient of AM.

Non-equilibrium Multi-Phase Field Model

In NEMPFM that is called as finite interface dissipation model [9], the reference volume (RV) is defined as small area in the phase field interface region. In practical calculation of discretized numerical method e.g. finite difference method, its grid is selected as RV, as illustrated in **Fig.1** It is assumed that diffusion is not considered between RVs. Concentration partition rate is assumed to be function of total free energy variation by concentration:

$$\dot{c}_\alpha^i \equiv -\sum_{j=1}^{n-1} \tilde{P}_\alpha^{ij} \frac{\delta G}{\delta c_\alpha^j},$$

(1)

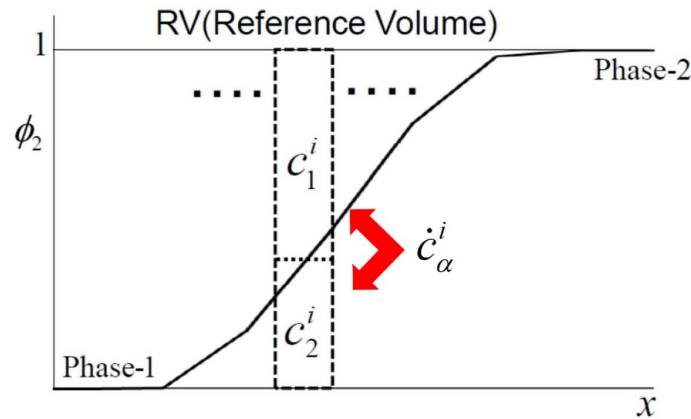**Fig.1** Reference volume definition in phase field interface region.

where c_α^i is the concentration of the i (i=C, Cr, Ni, Mo) atoms in α phases (α=liquid, FCC, BCC), G is the total energy of the system and $\tilde{P}_\alpha^{ij}$ is the interface permeability [9]. The other basic equations are the same as the standard multi-phase field method equations. However, Lagrange multiplier term is added to the total energy with consideration of conservation law:

$$\begin{cases} G = \int_V \left[\sum_{\alpha=1}^{N} \sum_{\beta=\alpha+1}^{N} -\frac{1}{2}\varepsilon_{\alpha\beta}^2 \nabla\phi_\alpha \cdot \nabla\phi_\beta + \sum_{\alpha=1}^{N} \sum_{\beta=\alpha+1}^{N} W_{\alpha\beta}\phi_\alpha \cdot \phi_\beta + \sum_{\alpha=1}^{N} \phi_\alpha f_\alpha(\vec{c}_\alpha) + \sum_{i=1}^{n-1} \lambda^i \left[c^i - \sum_{\alpha=1}^{N}(\phi_\alpha c_\alpha^i) \right] \right] dV, \\ c^i \equiv \sum_{\alpha=1}^{N}(\phi_\alpha c_\alpha^i), \end{cases}$$

(2)

where ϕ_α is the order parameter of the phase α (α=liquid, FCC, BCC). ϕ_α varies between zero and unit. f_α

(α=liquid, FCC, BCC) is the chemical free energy density of liquid, austenite and ferrite, respectively. Solving Lagrange multiplier λ^i by substituting Eq.(2) into Eq.(1) with considering definitions, $\tilde{P}_\alpha^{ij}(\phi_\alpha) \equiv P_\alpha^{ij}/\phi_\alpha$ and $P_\alpha^{ij} \equiv \delta_{ij}P_\alpha^{(i)}$, and the conservation, $\dot{c}^i = 0$ leads to the solute partition rate equation:

$$\dot{c}_\alpha^i = \sum_{\beta=1}^{N} P_{\alpha\beta}^i \phi_\beta \left(\tilde{\mu}_\beta^i - \tilde{\mu}_\alpha^i \right) - \sum_{\beta=1}^{N} \dot{\phi}_\beta \left(c_\beta^i - c_\alpha^i \right), \tag{3}$$

where $P_\alpha^{(i)}$ is represented as $P_{\alpha\beta}^i$ because the permeability parameter is defined in the interface between two phases as shown in **Fig.1**. $\tilde{\mu}_\alpha^i$ is diffusion potential that is defined as $\mu_\alpha^i - \mu_\alpha^{\text{Fe}}$, where μ_α^i and μ_α^{Fe} are chemical potential of phase α for solute i and solvent Fe, respectively. The first and the second terms in the right hand side of Eq.(3) work the diffusion potential difference effect and the interface moving effect terms, respectively. This partition rate equation is introduced instead of quasi-equilibrium partitioning calculation process of the standard multi-phase field method.

Parameters, $\varepsilon_{\alpha\beta}$ and $W_{\alpha\beta}$, in Eq.(2) are the gradient energy coefficient and the double-obstacle potential between αth and βth phases or grains, respectively. These parameters are given by relation with the interface energy $\sigma_{\alpha\beta}$ and the interface thickness δ [7] as:

$$\sigma_{\alpha\beta} = \frac{\pi}{4\sqrt{2}} \varepsilon_{\alpha\beta} \sqrt{W_{\alpha\beta}}, \tag{4}$$

$$\delta = \pi \frac{\varepsilon_{\alpha\beta}}{\sqrt{2W_{\alpha\beta}}}. \tag{5}$$

Substituting Eq.(2) into the time evolution equation (Allen-Cahn equation):

$$\frac{\partial \phi_\alpha}{\partial t} = -\sum_{j=1}^{N} \frac{M_{\alpha\beta}}{N} \left(\frac{\delta G}{\delta \phi_\alpha} - \frac{\delta G}{\delta \phi_\beta} \right), \tag{6}$$

with considering Eqs. (4) and (5) leads the following NEMPFM equation:

$$\frac{\partial \phi_\alpha}{\partial t} = \sum_{\beta=1}^{N} \frac{M_{\alpha\beta}}{N} \left\{ \sum_{\varsigma=1}^{N} \left[\left(\frac{\pi^2}{\delta^2} \phi_\varsigma + \nabla^2 \phi_\varsigma \right) \left(\sigma_{\beta\varsigma} - \sigma_{\alpha\varsigma} \right) \right] + \frac{2\pi}{\delta} \sqrt{\phi_\alpha \phi_\beta} \, \Delta G_{\alpha\beta} \right\}, \tag{7}$$

where $M_{\alpha\beta}$ is the interface mobility. $\Delta G_{\alpha\beta}$ is the interface driving force:

$$\Delta G_{\alpha\beta} = f_\beta - f_\alpha - \sum_{i=1}^{n-1} \left[\sum_{\varsigma=1}^{N} \phi_\varsigma \, \tilde{\mu}_\varsigma^i - \frac{1}{P_{\alpha\beta}^i} \sum_{\varsigma=1}^{N} \dot{\phi}_\varsigma c_\varsigma^i \right] \left(c_\beta^i - c_\alpha^i \right). \tag{8}$$

Eq.(8) is consistent with the driving force representation of the standard MPFM when $P_{\alpha\beta}^i$ becomes infinity. Free energy f_α, f_β and chemical potential μ_ς^i of phase α, β and ζ, respectively, are function of temperature and concentration in the interface region point. They are provided by TQ-interface calculation for CALPAH nonlinear polynomial formulation. This calculation consumes much time because its complex computation. Thus, in this study, TQ-interface calculation is replaced by simply linear computation of neural network prediction.

The diffusion equation is derived from substituting Eq.(2) into the time evolution equation of the conservation type, Cahn-Hilliard equation, as,

$$\frac{\partial c^k}{\partial t} = \nabla \left(\sum_{\alpha=1}^{N} \phi_\alpha \sum_{j=1}^{n-1} D_{kj}^\alpha \nabla c_\alpha^j \right),$$ (9)

where D_{kj}^α is diffusivity, of which value are given by Arrhenius-type data in this study. Eq.(8) are solved by coupling with Eq.(3).

Initial Composition and Thermal Conditions

In this study, calculations were performed in composition of duplex stainless steel 316L, Fe-18Cr-3Mo-12Ni-0.03C. We selected Thermo-Calc TCFE9 [13] for CALPHAD database. The equilibrium phase fractions for this initial composition system are shown in **Fig.2**. δ-ferrite and γ nucleates at 1727.8K and 1707.2K, respectively. δ-ferrite fraction increases before γ nucleation. After γ nucleation, δ-ferrite fraction, of which maximum value is about 65%, decreases with γ fraction increasing according to peritectic reaction. It is reported that γ nucleation was almost completely suppressed in high cooling rate of AM [14, 15] .
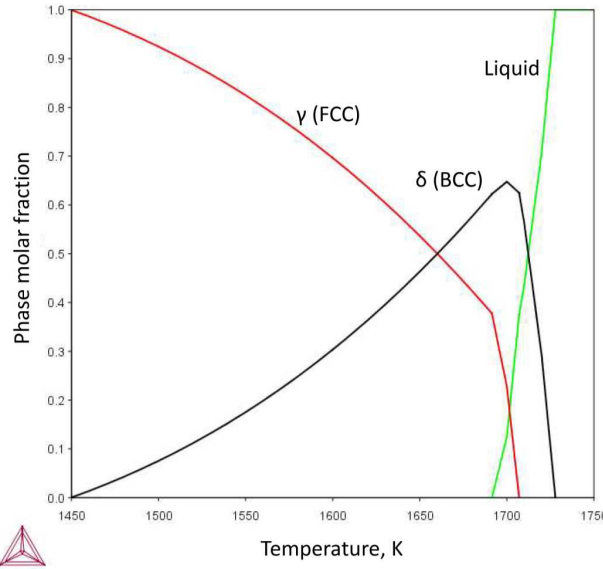

Fig.2 Equilibrium phase fractions of stainless steel 316L.

The neural network parameters, bias and weight values, of Gibbs free energy and chemical potential for liquid phase, δ-ferrite and γ were trained by solidification microstructure evolution of traditional casting conditions which were assumed for the cooling rate and the thermal gradient to be 25K/s and 400K/cm, respectively, which corresponded to continuous casting conditions [11]. This microstructure simulation was performed to compare with that of AM cooling rate and thermal gradient as well. However, the cooling rate and the thermal gradient in AM solidification depend on process type, laser or electron beam, process condition, powder material and so on. We assumed 10^5K/s and 10^4K/cm that were referred to approximate values of selective laser melting processing [15].

Machine Learning and Verification

The neural network of this study was designed as follows. Learning was performed for each phase, liquid, BCC(δ) and FCC(γ), individually. Number of input was five of temperature and four solute (Cr, Mo, Ni, C) molar

fractions for each phase. Number of output was six of Gibbs free energy density and five element (Cr, Fe, Mo, Ni, C) chemical potential values for each phase. Numbers of the hidden layer and its neuron were set as two and twenty, respectively. Sigmoid function and identify function were selected for the activation function of inner layer and for output layer, respectively.

Two dimensional finite difference method with explicit temporal integration, of which interval time was 1×10^{-5} s, was applied for the learning simulation. Calculation conditions of region size, grid size, number of grid, interface width, cooling rate, temperature gradient and boundary condition are shown **Fig.3**. The initial δ-ferrite nucleation was set in the left corner of the bottom. Initial temperature in the bottom was set as 1724K. It was defined for γ grain to nucleate in the interface region between liquid and δ-ferrite phases. Checking interval time and averaging distance of γ nucleation were set as 0.025s and 55.8μm, respectively. Physical parameter values, the interface energy and mobility, the interface permeability and diffusivity of Arrhenius plot data are shown in **Table 1**, **Table 2** and **Table 3**, respectively. The interface energy values were referred the article [16]. The interface mobility and the interface permeability values are decided by numerical examinations. The interface permeability was calibrated to obtain numerical stable condition by decreasing the parameter value from large one that caused numerical instability. The Arrhenius-type formulation data of the diffusivity were referring the diffusion mobility database MOBFE4 of Thermo-Calc software [17]. The training data were selected in time and space intervals as 0.01s (1000 time step) and 5μm (5 grid) for horizontal and vertical direction individually, respectively.
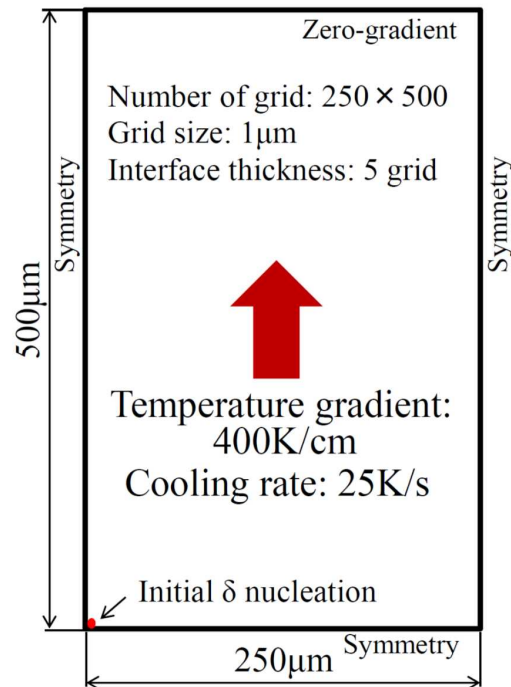

Fig.3 Calculation region conditions for machine learning.

Table 1 Interface energy and mobility [16].

Interface	energy	mobility
	J/m²	m⁴/J/s
δ - Liquid	0.2	1.5×10^{-10}
δ - γ	0.6	2×10^{-11}
Liquid − γ	0.2	3×10^{-11}

Table 2 Interface permeability.

Interface	m³/J/s			
	Cr	Mo	Ni	C
δ - Liquid				
δ - γ	2.5×10^{-7}	1.0×10^{-7}	1.0×10^{-7}	2.5×10^{-8}
Liquid − γ				

Table 3 Diffusivity of solute element (Arrhenius plot type) [17].

Phase	Element	Prefactor (m²/s)	Activation (J/mol)
Liquid	Cr	2×10^{-9}	0
	Mo	2×10^{-9}	0
	Ni	2×10^{-9}	0
	C	2×10^{-9}	0
γ(FCC)	Cr	7.830×10^{-5}	1.441×10^{5}
	Mo	7.883×10^{-6}	1.203×10^{5}
	Ni	4.128×10^{-5}	1.467×10^{5}
	C	4.915×10^{-3}	8.771×10^{4}
δ(BCC)	Cr	1.481×10^{-4}	1.055×10^{5}
	Mo	2.838×10^{-4}	1.133×10^{5}
	Ni	4.894×10^{-4}	1.123×10^{5}
	C	4.577×10^{-4}	3.800×10^{4}

The obtained neural network parameters, bias and weight values, were applied to NEMPFM program, of which the thermodynamics calculation part was replaced from TQ-Interface computation to the linear neural network procedure. **Fig.4** and **Fig.5** show C and Ni molar fraction distributions, respectively, with phase distribution of the direct CALPHAD database coupling (TQ-Interface) and the neural network prediction cases. In neural network case, the initial δ-ferrite nucleation was delayed about 10K because it seems for error of the obtained parameters to make the initial δ-ferrite nucleation driving force decreasing. However, δ-ferrite of the neural network case grows quickly after its nucleation by comparing of phase distributions between (a) and (b) of **Fig.4** or **Fig.5**. Nevertheless, morphology between (a) and (b) of **Fig.6** similar to each other, for examples, number of primary dendrite and primary dendrite tip curvature, except for detail. **Fig.6** shows phase fractions of the direct CALPHAD database coupling and the neural network parameter calculations versus to temperature. It can be seen for the δ-ferrite nucleation of neural network prediction case is delayed to direct database coupling one. The other hand, difference of δ-ferrite molar fraction between the neural network prediction and the direct database coupling cases decreases with temperature going down. It can be seen for phase fraction profiles to be good agreement between two cases, too. It is confirmed that thermodynamic calculation using neural network parameter provides similarity with direct database coupling one.

By comparing thermodynamics computation time between the neural network prediction and the direct database coupling cases, the former case was five times faster than the latter case. This means that this method has capability to be much faster by using highly parallel computer, e.g. GPU computer, because the linear neural network prediction procedure can be highly parallelized. Therefore, this neural network parameter method was applied to rapid solidification calculation of AM as following section.
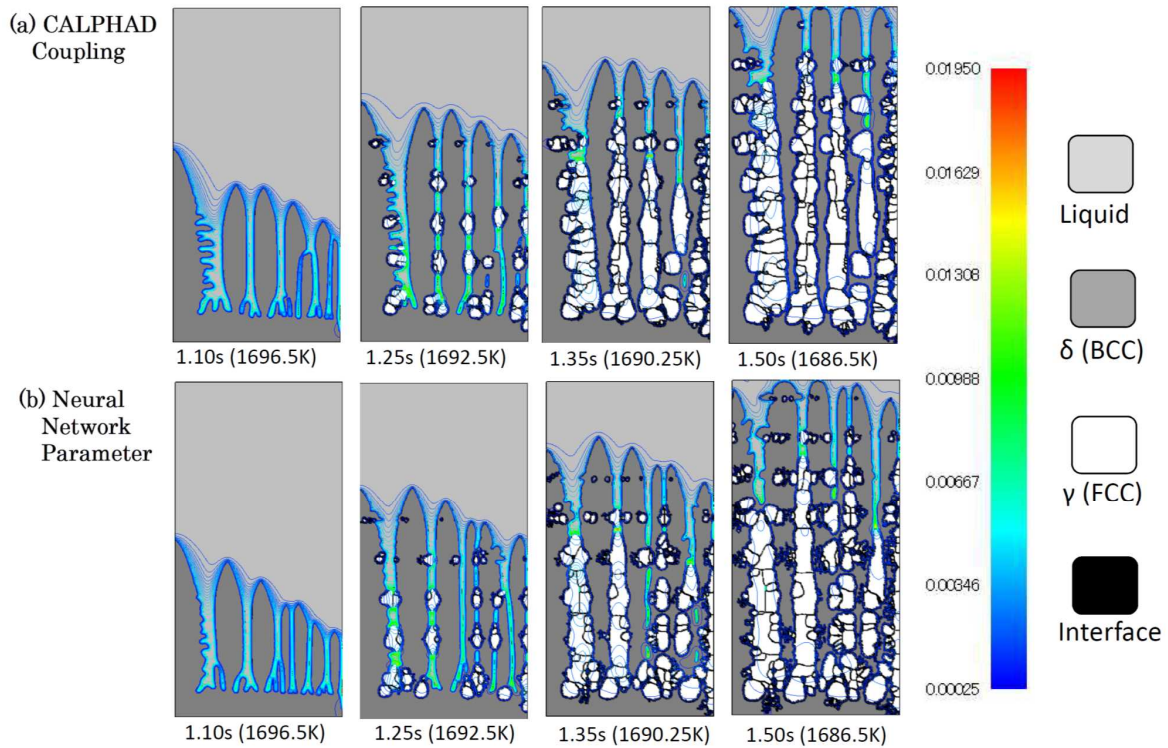
Fig.4 Snapshots of phase and C molar fraction distributions in calculation coupled with CALPHAD database and using neural network parameter.
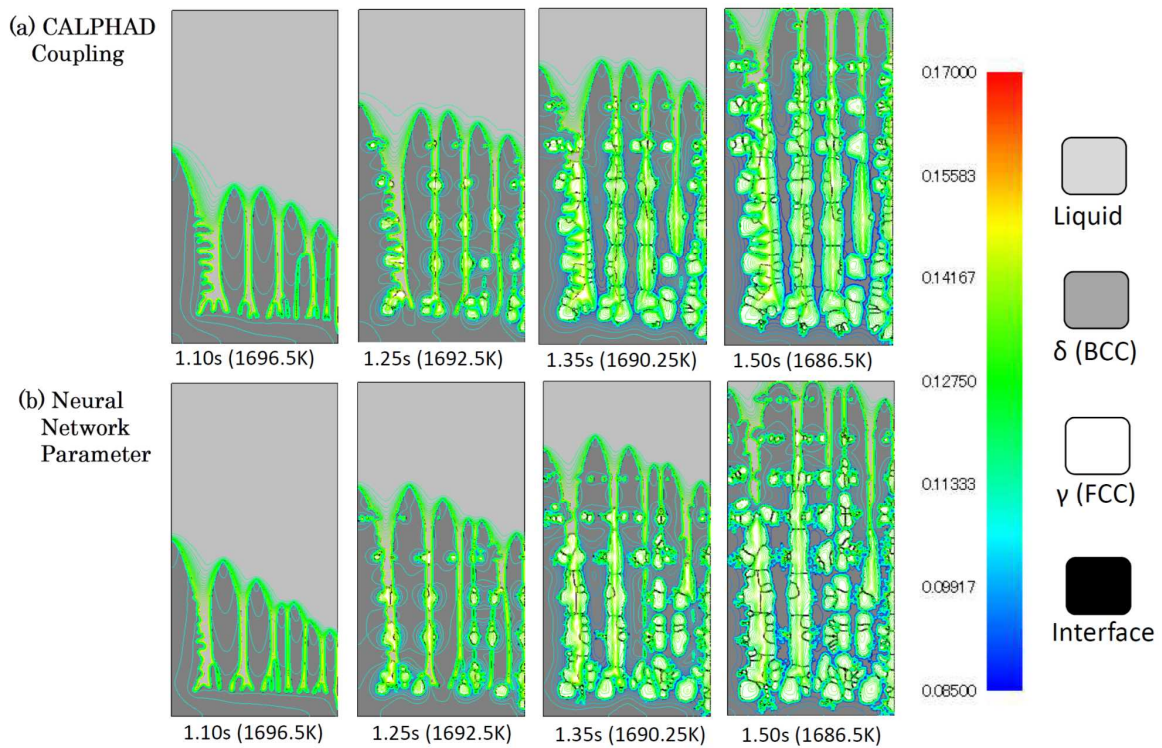

Fig.5 Snapshots of phase and Ni molar fraction distributions in calculation coupled with CALPHAD database and using neural network parameter.
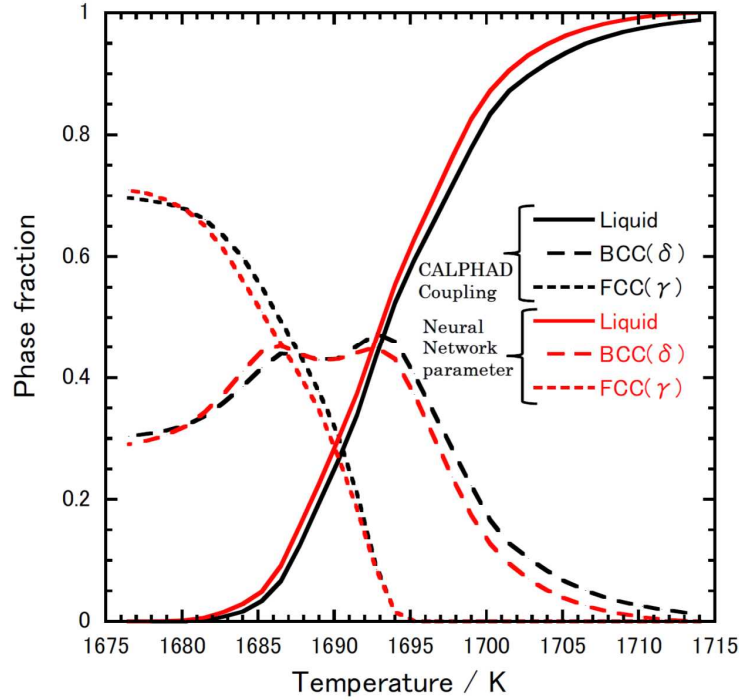
Fig.6 Comparison of phase fraction between directly CALPHAD database coupling (TQ-Interface) and the neural network parameter calculations.

Rapid Solidification for Additive Manufacturing Condition

Solidification simulation using the neural network parameter was performed in conditions of high cooling rate and thermal gradient, 10^5K/s and 10^4K/cm, respectively. Computation topology set as same as **Fig.3**. However, region and grid sizes should be reduced because the primary dendrite arm space size becomes shorter than that in conditions of 25K/s and 400K/cm. Primary dendrite arm space λ is generally represented with $\lambda = K\dot{T}^n$ [18], where K and n are constants depending on kind of alloy. Assuming $n = -0.5$, λ reduces two order by cooling rate changing from 25K/s 10^5K/s. The grid size is set to be 0.05µm in this case. The interval time was set as 2.5×10^{-8}s in order to maintain numerical stability for the grid size of the finite difference method. Calculation conditions is summarized in **Fig.7**. Number of grid was set as same as **Fig.3**. The same numbers of the surface energy and mobility (**Table 1**), the interface permeability (**Table 2**) and the diffusivity (**Table 3**) were applied to this simulation.
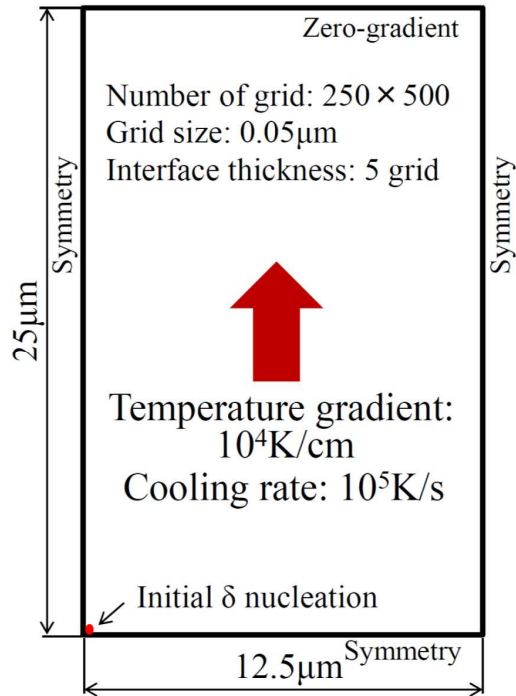
Fig.7 Calculation region conditions for rapid solidification AM.

In this rapid solidification condition, γ did not nucleate that was confirmed by experimental measurement [15]. Solute, Cr, Mo, Ni and C, molar fraction distributions are shown in **Fig.8**, **Fig.9**, **Fig.10** and **Fig.11**, respectively. It can be seen that solidification morphology behaves dendrite shape even if the cooling rate is extremely large. It means constitutional undercooling condition is held in this AM conditions. On the other hand, the dendritic morphology is very different between the high cooling rate (**Figs.8-11**) and low cooling rate (**Fig.4** or **Fig.5**). The secondary dendrite growth in **Figs.8-11** is more active by comparing with **Fig.4** or **Fig.5**. The primary dendrite arm space is approximately 3μm. The second dendrite arm space is shorter than the primary dendrite one. Element concentration partitioning also arises in interface between liquid and δ-ferrite. However, remained C concentration partitioning distribution in the δ-ferrite domain diffuses gradually, as seen in **Fig.11**. On the other hand, solute concentration values in bulk regions of liquid and δ-ferrite are almost same each other because the interface velocity is much faster than diffusion of not only substitutional element, Cr, Mo and Ni, but also interstitial element, C. NEMPFM using neural network parameter is conformed to be applied to AM rapid solidification computation.
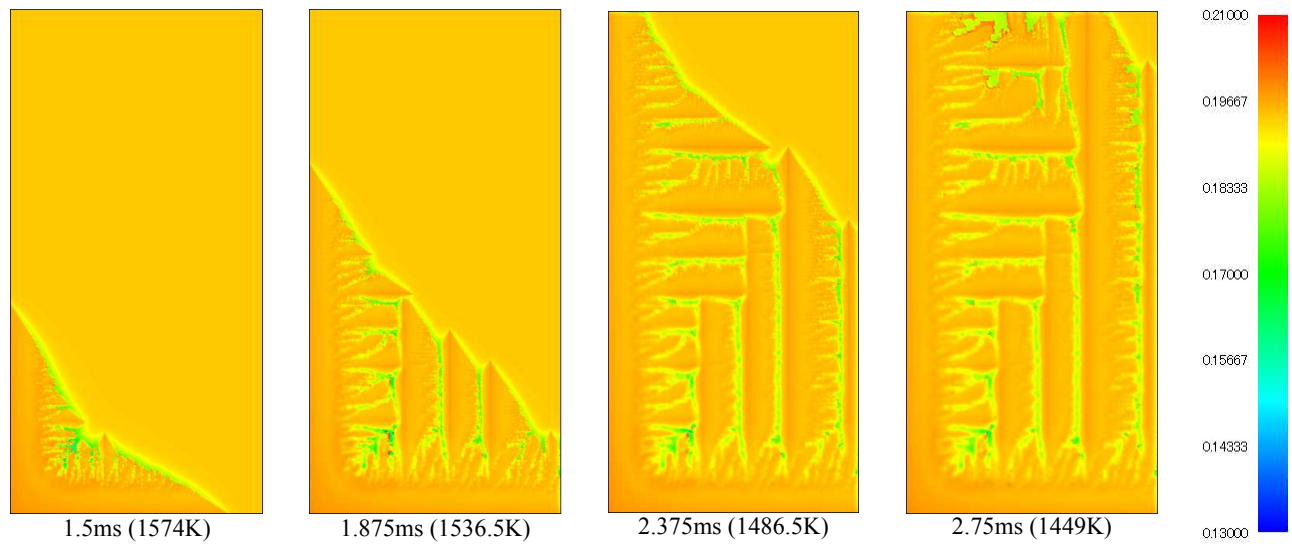
Fig.8 Snapshots of Cr fraction distributions in conditions of cooling rate, 10^5K/s, and thermal gradient, 10^4K/cm.
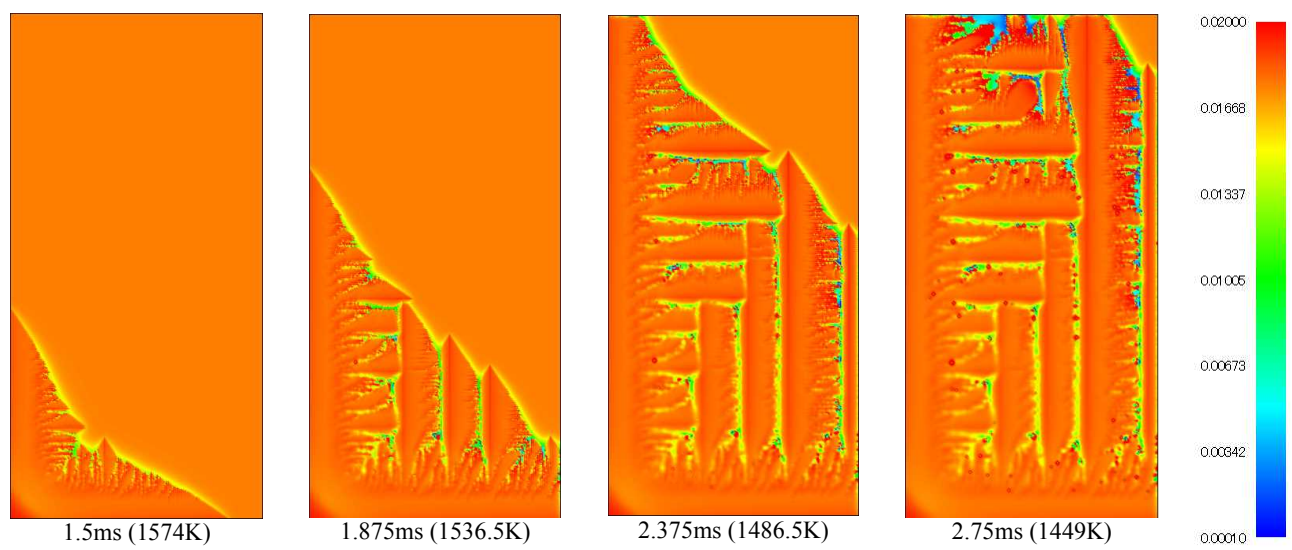

Fig.9 Snapshots of Mo fraction distributions in conditions of cooling rate, 10^5K/s, and thermal gradient, 10^4K/cm.
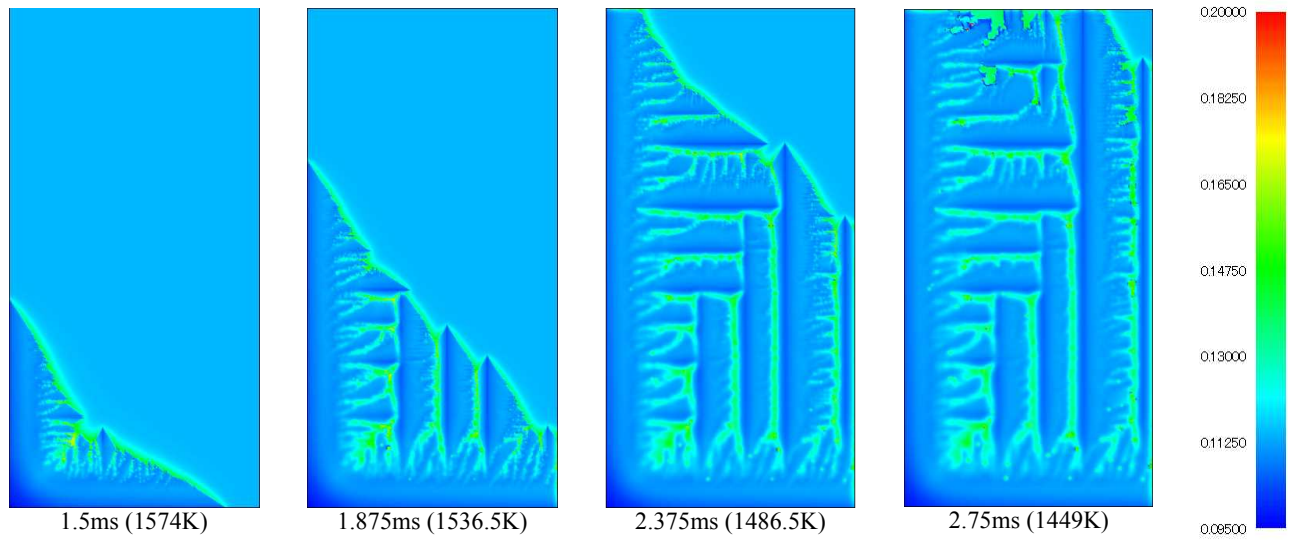
Fig.10 Snapshots of Ni fraction distributions in conditions of cooling rate, 10^5K/s, and thermal gradient, 10^4K/cm.
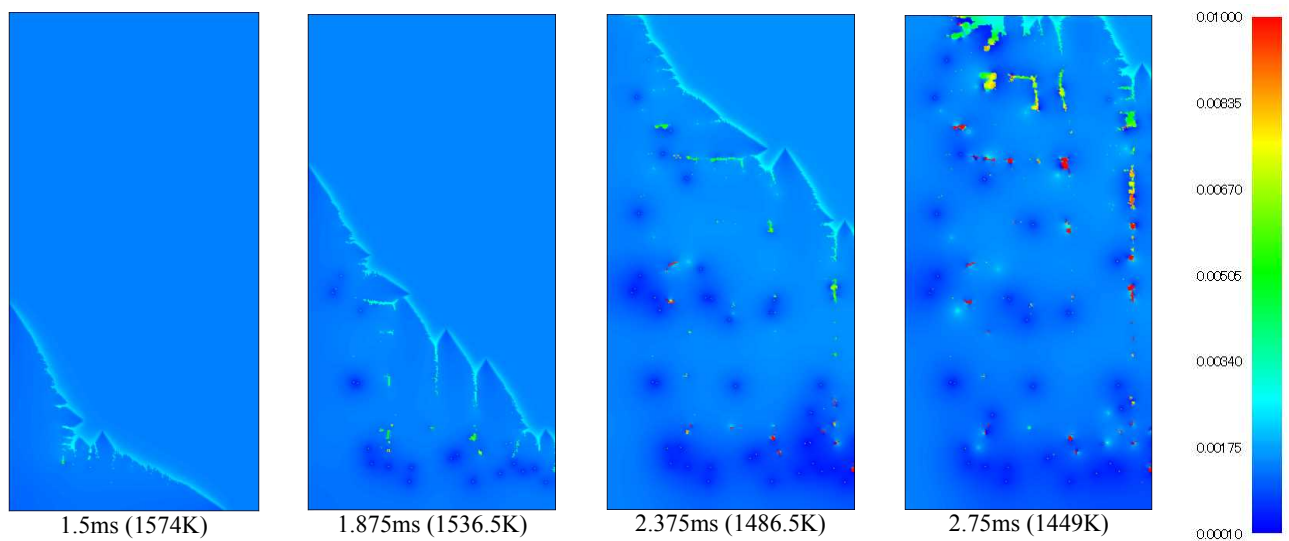

Fig.11 Snapshots of C fraction distributions in conditions of cooling rate, 10^5K/s, and thermal gradient, 10^4K/cm.

Conclusion

Non-equilibrium multi-phase field model program using neural network prediction procedure for thermodynamics has highly enough capability to simulate solidification microstructure evolution for multi component system in high cooling rate and thermal gradient of AM process conditions as well as traditional casting condition. This method provides high speed computation with no platform computer dependency.

References

[1]   J. Akram, P. Chalavadi, D. Pul and B. Stucker, "Understanding grain evolution in additive manufacturing through modeling", Additive Manufacturing, 21 (2018), 255–268.

[2] T. M. Rodges, J. D. Madison and V. Tikare, "Understanding grain evolution in additive manufacturing through modeling", Comp. Mater. Sci., 135 (2017), 78–89.

[3] S. Ghosh, L. Ma, N. O-. Opoku and J. E. Guyer,"On the primary spacing and microsegregation of cellular dendrites in laser deposited Ni Ni-Nb alloys", cond-mat. mtrl-sci, (2017)

[4] S.Ghosh, L. Ma, L. E. Levine, R. E. Ricker, M. R. Stoudt, J. C. Heigel and J. E. Guyer,"Sigle-Track Melt-Pool Measurements and Microstructures in Inconel 625", JOM, Technical Communication, (2018)

[5] I. Steinbach, *et al.*, "A phase field concept for multiphase systems," Physica D, 94 (1996), 135-147.

[6] http://www.thermocalc.com/products-services/software/software-development-kits/

[7] J.Eiken, B.Boettiger and I.Steinbach, "Multiphase-field approach for multicomponent alloys with extrapolation scheme for numerical application", Physical Review E, 73, 066122 (2006).

[8] S.G.Kim, W.T.Kim and T.Suzuki, "Phase-field model for binary alloys" Physical Review E, 60(1999), 7186-7197.

[9] I.Steinbach, L.Zhang and M.Plapp, "Phase-field model with finite interface dissipation", Acta Materialia, 60 (2012), 2689–2701.

[10] L.Zhang and I.Steinbach, "Phase-field model with finite interface dissipation: Extension to multi-component multi-phase alloys", Acta Materialia, 60 (2012), 2702–2710.

[11] S.Nomoto, K.Mori, M.Segawa and A.Yamanaka, "Solidification Simulation of Fe-C-Ni-Mo-C Duplex Stainless Steel using CALPHAD-coupled Multi-phase Field Model with Finite Interface Dissipation", *Proceedings of the 4th World Congress on Integrated Computational Materials Engineering (ICME2017)*, TMS, 283-292, 2017

[12] D. P. Kingma and L. J. Ba, "Adam: A Method for Stochastic Optimization", Conference paper at ICLR(2015), 13.

[13] http://www.thermocalc.com/products-services/software/software-development-kits/, 2017/6/26.

[14] K. Saeidi, L. Kevetkova, F. Lofaj and Z.Shen,"Novel ferritic stainless steel formed by laser melting from duplex stainless powder with advanced mechanical properties and high ductility", Mater. Sci. Eng. A, 665(2016) 59-65.

[15] F. Hengsbach, P. Koppa, K. Duschik, M. J. Holzweissig, M. Burns, J. Nellesen, W. Tillmann, T. Tröster, K-P. Hoyer and M. Schaper,"Duplex stainless fabricated by selective laser melting – Microstructure and mechanical properties", Materials and Design, 133(2017) 136-142.

[16] S.Fukumoto, Y. Ojkawa, S. Tsuge and S. Nomoto, "Prediction of Sigma Phase Formation in Fe–Cr–Ni–Mo–N Alloys", ISIJ International, 50 (2010), 445–449.

[17] http://www.thermocalc.com/products-services/databases/mobility/

[18] W. Kurz and D. J. Fisher,"Fundamentals of solidification", 4th revised edition, Trans Tech publications Ltd., 1998, p.84.